HHS Public Access

Author manuscript

Nat Med. Author manuscript; available in PMC 2015 October 01.

Published in final edited form as:

Nat Med. 2015 April ; 21(4): 373–382. doi:10.1038/nm.3826.

Activation of AMPKα2 in adipocytes is essential for nicotine-induced insulin resistance *in vivo*

Yue Wu[1,2], **Ping Song**[1], **Wencheng Zhang**[1], **Junhui Liu**[2], **Xiaoyan Dai**[1], **Zhaoyu Liu**[1], **Qiulun Lu**[1], **Changhan Ouyang**[1,3], **Zhonglin Xie**[1], **Zhengxing Zhao**[1], **Xiaozhen Zhuo**[2], **Benoit Viollet**[4,5,6], **Marc Foretz**[4,5,6], **Jiliang Wu**[3], **Zuyi Yuan**[2], and **Ming-Hui Zou**[1,3]

[1]Section of Molecular Medicine, Department of Medicine, University of Oklahoma Health Sciences Center, Oklahoma City, OK, USA

[2]Department of Cardiology, Cardiovascular Research Center, First Affiliated Hospital of Xi'an Jiaotong University, Xi'an, Shaanxi, China

[3]Key Laboratory of Hubei Province on Cardio-Cerebral Diseases, Hubei University of Science and Technology, Xianning, Hubei, China

[4]INSERM, U1016, Institut Cochin, Paris, France

[5]CNRS, UMR 8104, Paris, France

[6]Université Paris Descartes, Sorbonne Paris Cité, Paris, France

Abstract

Cigarette smoking promotes body weight reduction in humans while paradoxically also promoting insulin resistance (IR) and hyperinsulinemia. The mechanisms behind these effects of smoking are unclear. Here, we show that nicotine, a major constitute of cigarette smoke, selectively activates AMP-activated protein kinase α2 (AMPKα2) in adipocytes, which, in turn, phosphorylates MAP kinase phosphatase-1 (MKP1) at serine 334, initiating a proteasome-dependent degradation of this latter protein. The nicotine-dependent reduction in MKP1 induces the aberrant activation of p38 mitogen-activated protein kinase and c-Jun amino-terminal kinase leading to increased phosphorylation of insulin receptor substrate 1 (IRS1) at serine 307. This phosphorylation of IRS1 leads to its degradation, Akt inhibition, and the loss of insulin-mediated inhibition of lipolysis. Consequently, nicotine increases lipolysis, which results in body weight reduction, but this increase also elevates the levels of circulating free fatty acids and thus causes IR in insulin-

Correspondence should be addressed to: Ming-Hui Zou, M.D., Ph.D., BSEB 306, Department of Medicine, University of Oklahoma Health Sciences Center, 941 Stanton L. Young Blvd., Oklahoma City, OK 73104, USA, Phone: 405-271-3974, Fax: 405-271-3973, ming-hui-zou@ouhsc.edu.

AUTHOR CONTRIBUTIONS

Y.W. designed and performed the experiments, analyzed data, and drafted the manuscript. P.S., W.Z., X.D., Z.L., C.O., Z.X. and X.Z. performed a part of the animal experiments. J.L. and Z.Y. performed the human experiments. Z.Z. and J.W. partially performed the in vitro experiments, W.Z. and Q.L. generated series mutants. B.V. and M.F. provided the AMPK knockout mice. M.-H.Z. conceived the projects, designed the experiments, analyzed data, and wrote manuscript.

COMPETING FINANCIAL INTERESTS

The authors declare no competing financial interests.

sensitive tissues. These results newly place AMPKα2 as an essential mediator of nicotine-induced whole-body IR in spite of reductions in adiposity.

Keywords

Nicotine; insulin resistance; AMPK; MKP1; body weight

INTRODUCTION

Insulin resistance (IR) is a condition in which the body's cells become less sensitive to the effects of insulin, and higher levels of insulin are required to maintain its physiological functions. IR is often associated with obesity, inactivity, and excess body weight. In contrast, physical exercise and weight loss often lead to improved insulin sensitivity[1]. Nicotine, a major constituent of cigarette smoke, promotes hyperinsulinemia and IR – metabolic abnormalities that are typically associated with type 2 diabetes, cardiovascular disease, as well as with various cancers in smokers[2]. Paradoxically, cigarette smokers or individuals undergoing nicotine replacement therapy often have IR[3] even though they typically weigh less than nonsmokers[4]. This relationship is emphasized by the observation that when smokers cease smoking they undergo significant weight gain[4–6]. Indeed, long-term nicotine replacement therapy (nicotine gum) has been used as a method of weight control[3,7]. Importantly, replacement therapy has been reported to induce IR and metabolic disorders[3]. Highlighting this inverse relationship between IR and body weight in smokers, smoking cessation is linked to improvements in insulin sensitivity along with the significant weight gain that is often seen. The mechanism by which cigarette smoke or nicotine replacement therapy causes IR even in the presence of body weight reduction remains poorly understood.

The Jun N-terminal kinase (JNK) and the p38 protein kinases (p38) belong to the family of stress-activated protein kinases. JNK is activated by inflammatory cytokines, free fatty acids, cigarette smoke, and nicotine[8]. JNK is reported to suppress insulin signaling by causing phosphorylation of IRS1 at serine (Ser) 307 and subsequent Akt inhibition[9,10]. Further, JNK activity is abnormally elevated in obesity[11], and genetic ablation of JNK in mice results in decreased adiposity, improved insulin sensitivity, and enhanced insulin signaling[11]. Consistent with these findings, administration of a pharmacological inhibitor of JNK to leptin receptor-deficient *db/db* mice significantly improved their glucose levels[12], further supporting the notion that JNK is a key player in the development and progression of IR. Moreover, JNK was found to enhance lipolysis[13]. Despite reports that nicotine activates the p38-JNK signaling pathway in lung cancer cells[14], keratinocytes[15], and smooth muscle cells[16], there is currently no evidence supporting the *in vivo* activation of this pathway by nicotine or smoking. Thus, the molecular mechanisms by which nicotine activates the p38-JNK pathway, as well as inducing whole-body IR remain elusive.

AMP-activated protein kinase (AMPK) is a threonine/serine kinase that plays an important role in energy metabolism and is considered a cellular ‘fuel gauge’ and redox sensor. Evidence indicates that AMPK inhibition causes IR, whereas AMPK activation increases

insulin sensitivity[17,18]. Our previous studies reported that nicotine activates AMPK in both 3T3-L1-differentiated adipocytes and vascular smooth muscle cells[19,20]. Further, it has been reported that nicotine-induced weight loss is associated with the inactivation of hypothalamic AMPK in mice[21]. The aim of the present study was to evaluate whether AMPK activation in adipocytes contributes to the effects of nicotine on the development of IR in the face of body weight reduction. Here, we report that nicotine selectively activates AMPKα2 in adipocytes resulting in aberrant lipolysis that leads to a reduction in adiposity but also whole-body IR.

Results

Effects of nicotine on insulin resistance

To establish a causal relationship between nicotine, IR, and weight loss, nicotine (1.5 mg kg^{-1} day^{-1} for 6 weeks) was administered through osmotic minipumps subcutaneously implanted into 10-week-old high fat diet-treated C57BL/6J wild-type (WT) mice (Supplementary Fig. 1a). The average serum concentration of nicotine during treatment was 68 ± 5 ng/ml (Supplementary Fig. 1b), which is similar to the clinically relevant concentrations found in habitual cigarette smokers[22] or nicotine-containing chewing gum users[23]. As expected, nicotine infusion induced glucose intolerance and hyperinsulinemia (Fig. 1a). Insulin levels induced by glucose infusion were consistently and significantly higher in nicotine-treated mice than those in vehicle-treated mice (Fig. 1a). Likewise, nicotine-treated mice exhibited significantly elevated concentrations of glucose in an insulin tolerance test (ITT), compared to vehicle-treated mice (Fig. 1a). Consistently, in hyperinsulinemic-euglycemic clamp (H-E clamp) tests (Fig. 1b, Supplementary Fig. 1c), we found that nicotine-treated mice exhibited impaired glucose infusion rates (GIR) and increased hepatic glucose production (HGP) in parallel with decreased rates of glucose clearance (R_d), indicating that nicotine impairs hepatic insulin action and induces whole body IR.

Further, we examined the glucose metabolic index (R_g) in individual tissues during the H-E clamp test. Nicotine treatment resulted in lower R_g measurements in tibialis anterior and soleus muscles compared to vehicle-treated mice (Fig. 1b), indicating a nicotine-induced IR in skeletal muscle. Most strikingly, nicotine treatment corresponded with lower R_g measurements in epididymal white adipose tissue (eWAT) by 90% compared to vehicle-treated mice (Fig. 1c).

Nicotine decreases adiposity but promotes lipolysis in mice

Nicotine administration significantly resulted in lower body weight compared to vehicle-treated mice (Fig. 1d). We performed magnetic resonance imaging and found that nicotine treatment was significantly associated with less WAT compared to vehicle-treated mice (Fig. 1e). We further found that nicotine treatment resulted in less fat mass and smaller adipocyte size (83.5 μm vs. 49.3 μm in diameter), but unchanged lean body mass, compared to vehicle-treated mice (Fig. 1e,f), Moreover, compared to vehicle-treated mice nicotine did not change the temperature in the skin surrounding brown adipose tissue (BAT) or the rectal temperature (Fig. 1f).

Next, we investigated if smaller adipocytes observed in nicotine-treated mice resulted from enhanced lipolysis. Under fasting conditions, serum concentrations of free fatty acids (FFAs) were similar between vehicle- and nicotine-treated mice (Fig. 1g). Because insulin inhibits lipolysis[24], we assessed the effect of nicotine on insulin-mediated inhibition of lipolysis. We found that in vehicle-treated mice insulin perfusion resulted in significantly lower serum FFAs compared to insulin-perfused, nicotine-treated mice (Fig. 1g). Furthermore, in these experiments serum concentrations of FFAs negatively correlated with the fat mass in the mice (Fig. 1g). *In vivo* lipolysis assays demonstrated that nicotine treatment was associated with an attenuation of insulin-dependent inhibition of lipolysis (Fig. 1h). As the activation of phosphodiesterases (PDEs) is a prominent feature of insulin's anti-lipolytic effect, we next monitored the effects of nicotine on PDE activity. As expected, nicotine blocked insulin-induced PDE activation (Supplementary Fig. 1d). Although nicotine did not alter either basal or isoproterenol (ISO)-induced lipolysis in isolated adipocytes of WAT compared to vehicle treatment (Fig. 1i), nicotine treatment, compared to vehicle treatment, was significantly associated with less insulin-mediated inhibition of ISO-induced lipolysis (Fig. 1i). Moreover, nicotine treatment resulted in markedly higher liver triglydcerides (TG) and serum TG concentrations compared to vehicle treatment (Supplementary Fig. 1e). Taken together, these results indicate that nicotine promotes lipolysis.

It should be noted that, different from previous data using a high dose of nicotine[21,25], the clinically-relevant concentration of nicotine used here did not alter O_2 consumption (VO_2), CO_2 elimination (VCO_2), energy expenditure (EE), physical activity, or food intake compared to vehicle treatment (Supplementary Fig. 1f). We did see, however, that compared to vehicle treatment nicotine treatment was associated with slightly higher VO_2 in parallel with a modestly lower VCO_2, which resulted in markedly lower respiratory quotient (RQ) (Fig. 1j), indicating that nicotine induces fatty acid oxidation *in vivo*.

Acipimox lowers nicotine-induced FFA release and IR

Elevated levels of circulating FFAs are linked to IR[26,27]. To investigate if nicotine-induced lipolysis contributes to whole-body IR and low body weight, mice were simultaneously treated with nicotine and acipimox, a potent chemical inhibitor of lipolysis[28] (Supplementary Fig. 2a). Treatment with acipimox alone (0.08 g kg^{-1} day^{-1}) had no effects on body weight, fat mass, lean mass, serum insulin concentration, intraperitoneal glucose tolerance test (IPGTT), and ITT (data not shown). In addition, the co-administration of acipimox into nicotine-perfused mice did not alter serum nicotine concentrations, EE, VO_2, VCO_2, physical activity, or food intake when compared to mice treated with nicotine alone (Supplementary Fig. 2b,c). However, acipimox when co-administered with nicotine, blunted the ability of the latter to result in lower body weight (Fig. 2a), fat mass (Fig. 2b), adipocyte size (Fig. 2c) compared to vehicle treatment. Further, acipimox treatment also prevented the nicotine-induced higher serum FFAs (Fig. 2d) and hepatic and serum TG levels (Supplementary Fig. 2d), as well as the lower RQ measurement, compared to that seen in vehicle-treated mice (Fig. 2e). Since acipimox did not alter FFA uptake and esterification *in vivo* compared to vehicle-treated mice or nicotine-alone–treated mice (Supplementary Fig.

2e), these data suggest that nicotine-induced lipolysis is the key event linking decreased adiposity with increased fatty acid oxidation.

We performed IPGTTs and found that acipimox partially reversed nicotine-induced glucose intolerance (Fig. 2f). Acipimox also attenuated the effects of nicotine on insulin levels under fasting conditions (Fig. 2f), insulin release triggered by glucose injections (Fig. 2f) and IR (Fig. 2g). In an H-E clamp test (Fig. 1h,i and Supplementary Fig. 2f), acipimox significantly attenuated nicotine-induced IR and markedly improved the nicotine-dependent impairment of GIR (as compared to vehicle-treated mice) (Fig. 2h). Further, acipimox pronouncedly ablated the higher HGP levels, the inhibition of clamp R_d, and the reduction of R_g in tibialis anterior and soleus muscles seen in nicotine-treated mice *versus* vehicle-treated mice (Fig. 2i), indicating lipolysis inhibition by acipimox ablated nicotine-induced whole-body glucose intolerance and muscle and liver IR. In contrast, acipimox did not affect the lower R_g measurements in eWAT in nicotine-treated mice compared to vehicle-treated mice (Fig. 2i), consistent with the fact that WAT is not a primary site for FFA oxidation.

Next, we assayed the effects of nicotine on insulin signaling in WAT, skeletal muscle, and liver tissue. Acipimox abolished the nicotine-induced reduction (compared to vehicle treatment) of Irs1 protein in skeletal muscle and liver (Fig. 2j) but not in WAT (Fig. 2j). Nicotine suppressed insulin-stimulated Akt phosphorylation at Ser473 (pAkt) in skeletal muscle, liver, and WAT (Fig. 2j). Interestingly, acipimox attenuated these on pAkt in skeletal muscle and liver, but not in WAT (Fig. 2j).

Adipose AMPKα2 is required for nicotine-enhanced lipolysis

AMPK is a key energy and redox sensor[29] that plays a pivotal role in lipid metabolism[30] and insulin signaling[31,32]. AMPK activation by nicotine enhances lipolysis in 3T3L1-differentiated adipocytes[19], but the regulation of AMPK in lipolysis is controversial[33–37]. To establish a causative role of AMPK in nicotine-induced IR and enhanced lipolysis, AMPKα1-deficient (*Prkaa1*$^{-/-}$) and AMPKα2-deficient (*Prkaa2*$^{-/-}$) mice were treated with nicotine (Supplementary Fig. 3a). The serum nicotine concentrations and food intake in *Prkaa1*$^{-/-}$ mice and *Prkaa2*$^{-/-}$ mice were similar (Supplementary Fig. 3b–c). Compared to vehicle treatment, nicotine infusion significantly induced glucose intolerance, fasting insulin levels, glucose-induced insulin release, and insulin intolerance in *Prkaa1*$^{-/-}$ mice, but not in *Prkaa2*$^{-/-}$ mice (Fig. 3a–c). Furthermore, nicotine treatment was associated with significantly lower body weight and fat mass in *Prkaa1*$^{-/-}$ mice, but not in *Prkaa2*$^{-/-}$ mice, compared to vehicle control (Fig. 3d and Supplementary Fig. 3d). In addition, deficiency of AMPKα2, but not AMPKα1, prevented nicotine-induced WAT loss (Supplementary Fig. 3d), adipocyte size reduction (Fig. 3e), FFA elevation (Fig. 3f), and hepatic and serum TG elevation (Supplementary Fig. 3e).

In WAT, nicotine treatment was significantly associated with higher levels of phosphorylated AMPK (pAMPK) and acetyl-coA carboxylase (pACC) (Fig. 4a). ACC is a well-established AMPK substrate[30]. Interestingly, the levels of pAMPK after nicotine treatment (compared to vehicle treatment) were significantly greater in adipose tissues (11 fold) (Fig. 4a) than in the hypothalamus (1.1 fold), liver (2.3 fold) or muscle (1.8 fold) (Supplementary Fig. 3f).

As shown above, because nicotine resulted in significantly less fat mass compared to vehicle, it was important to determine if selective AMPKα2 deletion in WAT could prevent nicotine-induced IR and lipolysis. Consistent with a previous report using rat adipocytes[34], AMPKα1 was the major isoform (approximately 85%) of AMPKα, whereas AMPKα2 was the minor isoform (approximately 15%) in WAT (Fig. 4b). To determine the contribution of adipose AMPKα isoforms in nicotine-induced IR, we treated adipocyte-specific (via an *Adipoq-Cre* delete strain) AMPKα-knockout mice (*Prkaa1*$^{\Delta ad}$ and *Prkaa2*$^{\Delta ad}$), along with littermate control mice (Con), with nicotine (Supplementary Fig. 4a). The serum nicotine concentrations and food intake in the three groups were similar (Supplementary Fig. 4b–c). We found that nicotine treatment resulted in significantly less body weight in both Con and *Prkaa1*$^{\Delta ad}$ mice compared to vehicle treatment, but was without effect in *Prkaa2*$^{\Delta ad}$ mice (Fig. 4c). Furthermore, nicotine resulted in significantly less fat mass (Supplementary Fig. 4d) and adipocyte sizes (Fig. 4d) in Con and *Prkaa1*$^{\Delta ad}$ mice compared to vehicle treatment, but was also without effect on these parameters in *Prkaa2*$^{\Delta ad}$ mice (Supplementary Fig. 4d and Fig. 4d). Further, compared to vehicle treatment nicotine ablated the inhibitory effects of insulin on circulating FFAs (Fig. 4e) and *in vivo* lipolysis (Supplementary Fig. 5e) in both Con and *Prkaa1*$^{\Delta ad}$ mice, but not in *Prkaa2*$^{\Delta ad}$ mice, indicating that adipose AMPKα2 is responsible for WAT reduction and the aberrant lipolysis.

Nicotine induces insulin resistance through adipose AMPKα2

Treatment with nicotine dramatically impaired glucose tolerance (Fig. 4f), insulin sensitivity (Supplementary Fig. 4f), and glucose infusion-stimulated insulin release (Supplementary Fig. 4g) in Con and *Prkaa1*$^{\Delta ad}$ mice but not in *Prkaa2*$^{\Delta ad}$ mice. Moreover, nicotine was associated with lower Irs1 protein levels in WAT from Con and *Prkaa1*$^{\Delta ad}$ mice but not in that from *Prkaa2*$^{\Delta ad}$ mice (Fig. 4g). Consistent with this, nicotine attenuated insulin-stimulated phosphorylation of Akt at Ser473 in WAT from Con and *Prkaa1*$^{\Delta ad}$ mice but not in WAT from *Prkaa2*$^{\Delta ad}$ mice (Fig. 4g). Moreover, compared to vehicle nicotine induced a higher degree of Irs1 phosphorylation at Ser307 in an AMPKα2-dependent manner (Fig. 4g). Finally, nicotine decreased total Irs1 protein level without altering the *Irs1* mRNA level by RT-PCR (data not shown).

Besides regulation of Irs1 at Ser307 by the JNK-p38 signaling pathway, it is well established that mTOR- and S6K1-mediated phosphorylation of Irs1 at Ser636 and Ser639 leads to its inactivation and turnover[10,38,39]. Thus, we first assayed pS6K and pMtor with or without nicotine. We found that nicotine did not alter the levels of pS6K (Thr389) or pMtor (Ser2448) (Supplementary Fig. 5a). In line with this, nicotine did not alter the levels of pIrs1 at Ser636 or Ser639 (Supplementary Fig. 5a), two residues known to be phosphorylated by Mtor or S6K[10,39]. As nicotine did not alter the phosphorylation levels of Irs1 at Ser789 (Supplementary Fig. 5a), a reported phosphorylation site by SIK2 and AMPK[29,40], nicotine-enhanced phosphorylation of Irs1 at Ser307 (Fig. 4g) is unlikely due to direct AMPK phosphorylation of Irs1 as the phosphorylation of Ser789 would have likely then been affected also.

JNK is reported to suppress insulin signaling by causing phosphorylation of Irs1 at Ser307 and subsequent Akt inhibition[9,10]. We next tested the possibility that p38 or JNK activation

may mediate the phosphorylation and degradation of Irs1. We found that nicotine treatment resulted in markedly higher levels of p-p38 and pJNK in WAT from Con and *Prkaa1*$^{\Delta ad}$ mice, but not in WAT from *Prkaa2*$^{\Delta ad}$ mice (Fig. 4g). Moreover, selective JNK inhibition with JNK-IN-8 or p38 inhibition with SB203580 attenuated the nicotine-dependent phosphorylation of Irs1-Ser307 and the subsequent reduction of Irs1 protein expression (Supplementary Fig. 5b). Overall, these results indicate that adipose AMPKα2 is required for the nicotine-dependent upregulation of the p38-JNK pathway, and thus the subsequent increase in pIrs1, Irs1 degradation and Akt inhibition.

AMPKα2 alters the post-translational homeostasis of MKP1

MAP kinase phosphatase-1 (MKP1) (also known as Dusp1) is a well-characterized phosphatase that specifically negatively suppresses the p38-JNK pathway[41–43]. Therefore, we investigated the role of MKP1 in the nicotine-induced aberrant phosphorylation of p38 and JNK. Under baseline conditions, the expression of MKP1 in WAT was similar in all three mice models (Con, *Prkaa1*$^{\Delta ad}$ and *Prkaa2*$^{\Delta ad}$, Fig. 5a). However, nicotine resulted in markedly lower MKP1 protein levels in WAT of Con and *Prkaa1*$^{\Delta ad}$ mice but had no effect in WAT of *Prkaa2*$^{\Delta ad}$ mice (Fig. 5a). Interestingly, nicotine did not alter MKP1 mRNA levels in WAT (Fig. 5a), suggesting a post-translation modification is responsible for the nicotine-dependent reduction in MKP1 levels.

The stability of MKP-1 can be altered by phosphorylation. Next, we determined if nicotine treatment resulted in higher MKP1 phosphorylation at serine or threonine. We found that nicotine significantly induced MKP1 serine phosphorylation in an AMPKα2-dependent manner, but had no effect on threonine phosphorylation (Fig. 5a). Nicotine enhanced AMPKα2 binding with MKP1 in MEF-derived adipocytes (Fig. 5b). Further, nicotine dose- and time-dependently activated AMPK in isolated adipocytes as early as 1 hour (Fig. 5c and Supplementary Fig. 5c), induced MKP1 serine phosphorylation within 2 hours, and markedly lowered MKP1 protein level at 3 hours following the treatment compared to the levels seen at the initial time point (Fig. 5c). These data suggest that AMPK might directly phosphorylate MKP1 at a serine residue.

To this end, we analyzed all sequences around serine residues in the MKP1 protein (Supplementary Fig. 5d). Computer alignment with an optimal AMPK substrate motif yielded several potential AMPK phosphorylation sites in MKP1 including Ser131, Ser334, and Ser359 (Supplementary Fig. 5d,e). To further establish the roles of these potential phosphorylation sites in nicotine-induced MKP1 degradation, we generated three site-directed mutant constructs of MKP1 (so MKP1-S131A, -S334A, and -S359A). In HEK293 cells transfected with WT MKP1, stimulation with nicotine resulted in dramatically greater MKP1 serine phosphorylation compared to vehicle treatment (Fig. 5d). Nicotine-induced MKP1 serine phosphorylation was abolished only in cells transfected with MKP1-S334A, but not MKP1-S131A or -S359A, implying that Ser334 is the target of AMPK-mediated phosphorylation. Next, we performed an *in vitro* kinase assay with the peptides corresponding to residues 126–135, 329–338, and 354–363 of MKP1. The SAMS peptide, a canonical AMPK target sequence[29], was included as a positive control. We found that only peptide 329–338 of MKP1 was phosphorylated by the AMPKα2 protein (Fig. 5e).

Furthermore, mutation of serine to alanine at Ser6 of SAMS and Ser334 of MKP1 peptide 329–338 abolished AMPKα2-mediated phosphorylation, confirming that AMPKα2 directly phosphorylates MKP1 at Ser334.

We further determined whether AMPK-dependent MKP1 phosphorylation was required for the degradation of the MKP1 protein. To this end, we found that nicotine resulted in greater MKP1 polyubiquitination when compared to vehicle-treated cells, but that expression of MKP1-S334A did not result in appreciable ubiquitination of MKP1 (Fig. 5f). Moreover, we found that this nicotine-dependent MKP1 degradation was time-dependent (Fig. 5c) and that MG132, an inhibitor of the 26S proteasome, blocked this nicotine-induced MKP1 degradation (Fig. 5g). Taken together, these results imply that nicotine acts via AMPKα2 to phosphorylate MKP1 at Ser334, instigating MKP1 ubiquitination and proteasome-mediated degradation.

To further establish the role of MKP1 in nicotine-induced IR and lipolysis, adenoviruses encoding MKP1 or GFP were overexpressed in MEF-derived adipocytes. Compared with GFP controls, adenoviral overexpression of MKP1 ablated nicotine-induced p38 and JNK phosphorylation, blocked nicotine-induced Irs1 reduction, and reversed insulin-induced Akt phosphorylation (Fig. 5i). Moreover, MKP1 overexpression, but not GFP, abolished the inhibition of nicotine on insulin-suppressed lipolysis in MEF-derived adipocytes (Fig. 5i). These results suggest that reduction of MKP1 is a key step in nicotine-induced lipolysis and IR.

In isolated white adipocytes, nicotine induced the nuclear translocation of AMPKα2, but not AMPKα1 (Fig. 5h), which in turn mediated the degradation of nuclear protein MKP1 and the activation of p38 (Fig. 5h,i). In parallel, nicotine treatment dramatically increased the pMKP1-Ser334-dependent signal in WAT of Con and *Prkaa1*$^{\Delta ad}$ mice but not in that of *Prkaa2*$^{\Delta ad}$ mice *in vivo* (Fig. 5j). Taken together, these results support the notion that nicotine-induced nuclear-localized AMPKα2 phosphorylates MKP1 at Ser334, which instigates MKP1 degradation with consequent activation of the p38-JNK pathway.

MKP1 loss is required for nicotine-mediated IR and lipolysis

We next explored the *in vivo* relevance of the *in vitro* findings regarding MKP1 regulation by nicotine. We found that *Mkp1*$^{-/-}$ mice showed similar low body weights, low fat mass (Fig. 6a), enhanced *in vivo* lipolysis (Fig. 6b), and small WAT cell size (Supplementary Fig. 6a) as that observed in nicotine-treated mice. In addition, *Mkp1*$^{-/-}$ mice displayed a metabolic phenotype similar to that of nicotine-treated mice, including impaired glucose tolerance (Fig. 6c) and IR (Fig. 6d–f). Further, similar to nicotine-treated WT mice, *Mkp1*$^{-/-}$ mice exhibited elevated p38 activation, increased Irs1 phosphorylation at Ser307, and decreased Irs1 protein levels (Fig. 6g). Overall, these results imply that down regulation of MKP1 by activation of the p38-JNK pathway may cause enhanced lipolysis, low adiposity, and IR.

To further investigate the role of MKP1 in nicotine-induced IR *in vivo*, *Mkp1*$^{-/-}$ and WT mice were treated with vehicle or nicotine. The serum nicotine concentrations and food intake in WT and *Mkp1*$^{-/-}$ mice were similar (Supplementary Fig. 6b–c). In WT mice,

nicotine treatment correlated with lower body weight (Fig. 6a), fat mass (Fig. 6a and Supplementary Fig. 6d), and smaller WAT cell size (Supplementary Fig. 6a) compared to vehicle-treated mice, but was associated with higher FFA levels and greater lipolysis (Fig. 6b and Supplementary Fig. 6e,f). In contrast, in *Mkp1*$^{-/-}$ mice, nicotine did not alter body weights (Fig. 6a), fat mass (Fig. 6a), lipolysis (Fig. 6b), WAT cell size (Supplementary Fig. 8a) or glucose tolerance (Fig. 6c–f and Supplementary Fig. 6g, h) compared to vehicle-treated mice. Moreover, nicotine did not alter p38 activation, Irs1 phosphorylation at Ser307, and Irs1 protein level in *Mkp1*$^{-/-}$ mice compared to vehicle-treated mice (Fig. 6g). Taken together, these results suggest that MKP1 reduction is required for nicotine-mediated IR and lipolysis.

Nicotine receptor mediates nicotine-stimulated AMPK activation

Nicotinic acetylcholine receptor α7 subunit (AchRα7) is the major receptor for nicotine[44,45]. To establish the role of AchRα7 in nicotine-enhanced AMPK activation, we knocked down AchRα7 expression in adipocytes using a AchRα7-specific lentivirus shRNA. We found that in a time-dependent manner nicotine was associated with higher reactive oxygen species (ROS), pAMPK levels, and lower MKP1 protein levels in MEF-derived adipocytes compared to the initial time point, and that knockdown of AchRα7 abolished these effects (Supplementary Fig. 7a).

Further, we detected AchRα7 expression in isolated adipocytes, hepatocytes, β-cells, and myocytes from wild-type mice. We found that the highest amounts of AchRα7 were in the adipocytes and that nicotine had a more pronounced effect on ROS production, AMPK activation, and MKP1 expression in these cells compared to those from the other tissues (Fig. 6h).

Next, we assessed whether other activators of AMPKα2 alter MKP1 expression and lipolysis in cultured adipocytes. We found that clinically relevant concentrations of metformin (2–20 μM) had marginal effects in adipocytes on MKP1 expression compared to the strong effects that nicotine has on lowering MKP1 levels (Supplementary Fig. 7b). However, high concentrations of metformin (2 mM) did result in markedly greater pAMPK levels, lower MKP1 levels, and reversed insulin-blocked lipolysis (Supplementary Fig. 7b). Additionally, ROS scavengers or inhibition of ROS production abolished nicotine-induced AMPK activation (Supplementary Fig. 7c), indicating that nicotine activates AMPKα2 through ROS induction.

Nicotine-induced lipolysis and IR occurs in smokers and rats

It was important to investigate if nicotine activated AMPK-MKP1-IRS1 signaling in the adipose tissue of smokers. We found higher pAMPK, and lower MKP1 and IRS1 in WAT in smokers compared to nonsmokers. Moreover, the blood glucose and plasma insulin response during an oral glucose tolerance test (OGTT) was significantly higher in smokers than nonsmokers (Fig. 6j). Additionally, smokers showed lower fat percentage, higher serum FFA levels, and a higher degree of lipolysis than that observed in nonsmokers (Supplementary Fig. 7d–f and Supplementary Table 1).

Finally, there is evidence that that low dose nicotine (1.5 mg kg^{-1} day^{-1}) in mice induces lipolysis and hepatic steatosis[46]. In contrast, others report that in rats, high dose of nicotine (3–4 mg kg^{-1} day^{-1}, equal to 6–8 mg kg^{-1} day^{-1} in mice) alleviates IR *via* severe weight loss, negative energy balance, increased locomotor activity, and elevated BAT thermogenesis[21,47,48]. To address the discrepancy between mice and rats, we investigated the metabolic effects of low dose (0.8 mg kg^{-1} day^{-1}, equal to 1.5 mg kg^{-1} day^{-1} in mice) and high dose (4 mg kg^{-1} day^{-1}) of nicotine on rats. As shown in Supplementary Fig. 8a–c, the low dose of nicotine (similar to clinical concentration in smokers) induced both IR and mild body weight loss, whereas the high dose of nicotine induced severe body weight loss with improved glucose tolerance in rats.

Discussion

This study has shown, for what we believe is the first time, that AMPKα2, but not AMPKα1, is essential for nicotine-induced IR and aberrant lipolysis in WAT of mice *in vivo*. Mechanistically, we demonstrate that nicotine via elevation of ROS levels selectively activates adipose AMPKα2, which phosphorylates MKP1 at Ser334, leading to the ubiquitination-mediated degradation of MKP1. MKP1 reduction consequently results in aberrant p38-JNK activation, which mediates Irs1 phosphorylation at Ser307 resulting in its degradation, and subsequent inhibition of Akt phosphorylation at Ser473. As a result, nicotine impairs insulin signaling in WAT, upregulates lipolysis, and elevates circulating FFA levels. This increase in circulating FFAs, in turn, impairs insulin sensitivity in other insulin-sensitive tissues, such as skeletal muscle and liver (Supplementary Fig. 8d). Of note, nicotine considerably increases the levels of hepatic and serum triglycerides (TG) and circulating FFAs, and promotes liver steatosis, all of which are ablated by lipolysis inhibition with acipimox. These results indicate that nicotine promotes lipid redistribution from fats into other organs and circulating blood, which contributes to the development of insulin resistance.

Although AMPK-induced activation of the p38-JNK pathway has been reported in different cell types[17,18,49], the mechanism for this regulation remained unclear. Here, we have demonstrated that AMPK-dependent MKP1 degradation is required for AMPK-mediated activation of the p38-JNK pathway. We showed that MKP1 is phosphorylated by AMPK at Ser334 and this phosphorylation results in its ubiquitiation-dependent degradation. Indeed, MKP1 has been reported to be susceptible to ubiquitiation and degradation[50]. *Mkp1*$^{-/-}$ mice display low body weight, small WAT and adipocyte size, enhanced p38-JNK activation, delayed insulin-induced pAkt in adipocytes, and elevated glucose in IPGTT[43], all of which are similar to nicotine-treated mice. Intriguingly, AMPK can phosphorylate different proteins to exert broad functions in multiple cellular types. For example, AP-2α is phosphorylated by AMPK at Ser212 in smooth muscle cells resulting in aberrant expression of matrix metalloproteinase[20].

Several studies indicate that AMPK activation induces weight loss. First, AMPK activation is reported to inhibit insulin-mediated, anti-lipolysis-required IRS-Akt signaling[31,51]. Second, *Prkaa1*$^{-/-}$ mice exhibit low body weight and decreased adipocyte cell size[34], which may be due to the compensatory effects of AMPKα2 over-activation. Third, high-fat diet-

treated *Prkaa2*$^{-/-}$ mice exhibit increased body weight, WAT mass, and adipocyte size[52] indicating an AMPKα2-dependent effect on lipolysis in adipose tissues. Finally, nicotine-activated AMPK induces lipolysis and blocks fatty acid synthase in 3T3-L1 adipocytes[19]. These effects of AMPK appear to be independent of the activation of Sirt1 and PGC-1α, two known targets of AMPK in IR[17,18].

Insulin is known to block lipolysis, increase body weight[53,54], activate IRS-Akt signaling, and inhibit AMPK signaling[31]. Another important implication of the present study is that IR in adipocytes (that is, the suppression of insulin-induced inhibition of lipolysis) is required for whole-body IR and adiposity reduction in cigarette smokers and in patients with nicotine replacement therapy. This notion is supported by the fact that nicotine had little effect on IR or adiposity reduction in *Prkaa2*$^{\Delta ad}$ mice. Further, nicotine suppresses the effects of insulin-blocked lipolysis despite that nicotine alone did not affect basal lipolysis in adipocytes. Importantly, the inhibition of lipolysis-normalized insulin sensitivity in skeletal muscle but not in adipose tissues, suggesting that IR in skeletal muscle results from the elevation of circulating FFAs in nicotine-treated mice. Moreover, anti-lypolytic drugs such as acipimox might be beneficial in treating IR in cigarette smokers or those undergoing nicotine replacement therapy. Finally, we have found that AMPK in WAT is preferentially targeted by nicotine. This skewing likely results from the relatively higher expression of the nicotine receptor, AchRα7, in WAT compared with other tissue types and the high lipophilicity of nicotine, which would lead to its accumulation in the adipose tissue[55].

In summary, the data here shows that AMPKα2 is essential for nicotine-induced lipolysis and whole body IR. Our results might help explain the paradoxical links of body weight loss and whole body IR in cigarette smokers. Additionally, the results also suggest that anti-lypolytic drugs such as acipimox might be useful for treating IR in smokers or in patients undergoing nicotine-based smoking cessation therapy.

ONLINE METHODS

Animals

Prkaa1$^{-/-}$, *Prkaa2*$^{-/-}$ and *Mkp1*$^{-/-}$ mice were generated as previously described[56,57]. *Prkaa1*$^{flox/flox}$ and *Prkaa2*$^{flox/flox}$ mice (provided by Dr. Benoit Viollet, Paris, France) were crossed with *Adipoq-Cre* mice (Jackson Laboratory, Stock Number: 010803) to generate adipose-specific knockout mice. All mice (male, 8 week old) were in the C57BL/6J background and housed in temperature-controlled cages with a 12-h light-dark cycle and given free access to water and food. The animal protocol was reviewed and approved by the Institutional Animal Care and Use Committee at the University of Oklahoma Health Sciences Center.

Eight week old male mice were randomized to receive infusion with nicotine (1.5 mg kg^{-1} day^{-1}, 6 weeks, N3876, Sigma) or saline (vehicle) using Alzet osmotic pumps (DURECT Corp.). Briefly, after mice were anesthetized with an intraperitoneal injection of ketamine (80 mg kg^{-1}) and xylazine (5 mg kg^{-1}), pumps were placed into the subcutaneous space of anesthetized mice through a small incision in the back of the neck that was closed with sutures. All incision sites healed rapidly without any infection. Mice were fed with high-fat

diet (HFD, D12492, 60% fat; Research Diets, NJ) in the presence or absence of acipimox (0.08 g kg^{-1} day^{-1} in the drinking water, Sigma) for 5 weeks. For the intraperitoneal glucose tolerance test (IpGTT; overnight fasting mice injected with 1g kg^{-1} of glucose) and insulin tolerance test (ITT; 3-hours fasting mice injected with 1 unit kg^{-1} of insulin), mice were sacrificed 10 min after receiving intraperitoneal injections of insulin (1 unit kg^{-1}), then liver, muscle, and WAT were isolated for biochemical analyses. Male 10-week old Sprague-Dawley rats were randomized to receive infusion with low dose of nicotine (0.8 mg kg^{-1} day^{-1}), high dose of nicotine (4 mg kg^{-1} day^{-1}), or saline (vehicle) using Alzet osmotic pumps for 4 weeks and fed with chow diet. IPGTT (overnight fasting injected with 2g kg^{-1} of glucose) were performed in each group.

Hyperinsulinemic-euglycemic clamp

As previously described[58], catheters were implanted and the mice were allowed to recover for 5–7 days. After a 3-hour fast, [3-^{3}H] glucose (Perkin-Elmer, 0.075 μCi min^{-1}) was continuously infused for 2 h to assess basal glucose turnover, followed by hyperinsulinemic-euglycemic clamp for 130 min with primed-continuous infusion of human insulin (60 mU kg^{-1} bolus, 2.5 mU kg^{-1} min^{-1}, Humulin R; Eli Lilly, Indianapolis, IN), a continuous infusion of [^{3}H]glucose (0.15 μCi min^{-1}) and a variable infusion of 20% dextrose to maintain euglycemia (100–120 mg dl^{-1}). We obtained blood samples from the tail and measured tissue-specific glucose uptake after an injection of a bolus of 12 μCi of 2-deoxy-D-[1-^{14}C] glucose (Perkin Elmer) at 120 min. The results were then analyzed, as previously described[58,59].

Body composition analysis and temperature measurement

Body composition was determined with the nuclear magnetic resonance system using a Body Composition Analyzer Echo 900 (Echo Medical Systems, Houston, TX). Body temperature was recorded with a rectal probe connected to a digital thermometer (ReliOn, Waukegan, IL). Skin temperature surrounding BAT was recorded with an infrared camera and analyzed with a specific software package (A325sc: Compact-Infrared-Thermal-Imaging-Camera; FLIR, West Malling, Kent, U.K.)

Comprehensive metabolic monitoring

The metabolic rate of mice was measured by indirect calorimetry measurements using Comprehensive Laboratory Animal Monitoring Systems (Columbus Instruments, Columbus, OH). Mice of both genotypes were housed individually, acclimatized to respiratory chambers for 24 hours, and allowed free access to food and water. The data for VO_2, VCO_2, and locomotor activity were recorded in real time. Energy expenditure (kcal kg^{-1} h^{-1}) was calculated with the following formula: $(3.815\times VO_2 + 1.232 \times VCO_2)/1000$, and the respiratory quotient (RQ) was calculated by $RQ = VCO_2/VO_2$.

Pathological analysis of adipose tissue

Three-dimensional magnetic resonance imaging (3D MRI) was performed as previously described[60]. Tissues were fixed, embedded, and then stained according to standard procedures that have been described previously[61]. The diameter of adipocytes was measured

using Image Pro Plus software (Media.). A frequency distribution plot of cell diameters was used to determine the mean diameter of fat cells.

Processing adipose tissue samples from smokers and nonsmokers

WAT biopsies were obtained from 12 smokers and 12 nonsmokers (control). The demographic data are listed in Supplementary Table 1. Each subject underwent OGTT and insulin-releasing tests, as previously described[62]. Smoking index is equal to years of smoking × amount of smoking per day. Body fat percentage measurements were taken using the body fat analyzer (Omron). Subcutaneous WATs were collected from the participants through surgery with small incisions. This study complied with the Declaration of Helsinki, and informed consent was obtained from each participant. The research protocol was approved by the Ethics Committee of Xi'an Jiaotong University.

Assays for cholesterol, triglyceride, FFA, insulin, and nicotine

Fasting serum cholesterol and triglyceride levels were measured using reagents (Thermo Scientific) as previously described[61]. Serum insulin levels were measured at 0, 20, and 90 min of IpGTT by enzyme-linked immunoassay (ELISA) (ALPCO, Wandham, MA). Serum FFA levels were measured after overnight fasting or insulin perfusion at 40 min during ITT using an enzyme kit (Biovision, Mountain View, CA). Nicotine concentrations were measured according to the manufacturer's instructions (Abnova, Taiwan).

Phosphodiesterases (PDE) activity

Isolated adipocytes were pre-treated with nicotine (Nic, 300nM) or vehicles (Veh) for 4h. After being incubated with insulin for 10 min, the cells were assayed for PDE activity (PDE Activity Assay Kit, Abcam, ab139460), according to the instruction from the supplier.

Western blot analysis and immunoprecipitation (IP) assay

Antibodies against AMPK-α (2532), AMPK-α1 (2795), AMPK-α2(2757), pAMPK (Thr172, 2535), pACC (Ser79, 3661), ACC (3662), p38 (9212), pp38 (4631), JNK (9258), pJNK (9251), pIRS1 (Ser307, 2381), pIRS1 (Ser636/639, 2388), pIRS1 (Ser789, 2389), p-mTOR (Ser2448, 5536), mTOR (2983), pS6K (Thr389, 9324), S6K (2708), pRaptor (Ser789, 2083), Raptor (2280), pThr (9386) and histone H3 (9717) were purchased from Cell Signaling Technology. Antibodies to lactate dehydrogenase (LDH, SC-133123), Ub (SC-8017), MKP1 (SC-370), AchRα7 (SC-5544), Gapdh (SC-48166) and β-actin (SC-1616) were obtained from Santa Cruz Biotechnology. Antibodies to serine phosphorylation (pSer, Ab7851) were obtained from Abcam. IRS1 (06-284) was from Sigma. The polyclonal antibody against pMKP1--Ser334 [RGT(pSer)TTTVFNFPVS] was developed by immunizing sheep, then collecting and affinity purifying the antisera (performed by Genscript, NJ, USA) for the Western blot usage. We ran identical protein extracts in parallel on separate gels as technical replicates. We then transferred the gels to nylon membranes and cut the membranes into appropriate sections according to the expected molecular weight of the proteins of interest in that region. We then probed these separate membranes with the appropriate primary antibody. For proteins that ran very close together (such as the non-phosphorylated and phosphorylated version of a protein) we probed, then stripped and

reprobed for the related band. In some instances, though, the stripping and reprobing process reduced the subsequent signal of the next protein of interest. In those cases we probed the same region of the membrane from the other gel run in parallel. Western blot analysis and immunoprecipitation were performed as described previously[19]. We ran identical protein extracts in parallel on separate gels as technical replicates. We then transferred the gels to nylon membranes and cut the membranes into appropriate sections according to the expected molecular weight of the proteins of interest in that region. We then probed these separate membranes with the appropriate primary antibody. For proteins that ran very close together (such as the non-phosphorylated and phosphorylated version of a protein) we probed, then stripped and reprobed for the related bands. In some instances, though, the stripping and reprobing process reduced the subsequent signal of the next protein of interest. In those cases we probed the same region of the membrane from the other gel run in parallel.

Palmitate uptake and esterification

For measurements of palmitate uptake and esterification in WAT, methodology was adapted from previously detailed studies[63,64]. Briefly, [^{3}H] palmitate was tail-vein injected (100 μCi per mouse complexed to fatty acid-free bovine serum albumin) into mice. At 60 min following injection, mice were euthanized, blood samples were taken and WAT tissues were quickly excised, weighed and frozen at −80 °C until processing. Lipids were then extracted using a chloroform-to-methanol based extraction method. The radioactivity content of tissues was quantified as described previously[64], and the palmitate incorporation into esterified lipids was evaluated as described previously[63].

Lipolysis assays

Adipocytes were isolated from epididymal fat pads by collagenase digestion, and the lipolysis assay was performed as previously described[19,34]. Briefly, adipocytes (10^6 cells) were incubated at 37°C for 1h in 2.5 ml Krebs Ringer bicarbonate buffer (pH 7.4) containing 4% bovine serum albumin in 5% CO_2. They were then treated with or without insulin for 10 min, followed by a 90 min treatment with 10 μM isoproterenol (ISO). Subsequently, 1 ml of the incubation buffer of adipocytes was removed and acidified with 100 μl 30% trichloroacetic acid. The mixture was vigorously shaken and then centrifuged at 3000 g for 10 min at 4°C. The supernatant (100 μl) was collected and neutralized with 10 μl 10% KOH, after which it was assayed for glycerol content (Glycerol Kit, Sigma). The results are expressed in μg glycerol released per 100 mg lipids. For the MEF-differentiated adipocytes[65], the results are expressed in μg glycerol released per mg protein. For *in vivo* lipolysis, mice were fasted for 3 h and treated with an intraperitoneal injection of the β3-adrenergic receptor agonist CL-316243 (0.1 mg kg^{-1}) after 5 min insulin (0.6 unit kg^{-1}) or saline injectin. Blood was withdrawn from the tail at 0, 15, 60, 120 min after injection for determination of non-esterified fatty acid and glycerol levels.

Lentiviral shRNA transfection and adenoviral infections

Lentiviral-based AchRα7 shRNA, and control shRNA were obtained from Santz Cruz Biotechnology, and transfections were carried out according to the manufacturer's protocol. Ad-GFP and Ad-MKP1 transfections were performed as previously described[65].

Generation of DNA Constructs

Wild type MKP1 cDNA were purchased from Origene Company. S131, S334, or S359 of MKP1 was mutated to Alanine by using the QuikChange kit (Stratagene), according to the manufacturer's instructions[20,66]. Oligonucleotides used for point mutation are listed in Supplementary Tab. 2. All mutations were confirmed by DNA sequencing. Plasmid DNA was extracted on a large scale using Qiagen's EndoFree plasmid maxikit (cat. No. 12362) and transfected into HEK293 cells by using the Lipofectamine 2000 kit (Invitrogen, catalog no. 11668-019), according to the instructions provided by the supplier. After transfection, cells underwent 24-h incubation before receiving any additional treatments. Cells transfected with the expression vector as well as untreated cells served as controls.

In vitro kinase assays

According to a previous description[66], recombinant AMPKα2 peptides or the SAMS peptide (200 μM) were incubated in a kinase HEPES-Brij buffer containing 5 mM $MgCl_2$, 0.2 mM ATP with P^{32}-labeled ATP (1 μCi) for 15 min at 37°C with or without AMP (200 μM). The reaction mixture was supplemented with 20 μl of 3× sample buffer to terminate the reaction, boiled for 5 min at 95°C, and separated by SDS-PAGE. The dried gels were subjected to autoradiography to analyze changes in protein phosphorylation. Aliquots of the reaction mixture were also subjected to scintillation counting to determine AMPK activity, or more specifically, ^{32}P incorporation into the SAMS peptide. MKP1 peptides corresponding to residues 126–135, 329–343, 354–363 and the SAMS peptide were generated by Genescript Company. The phosphorylation bands were visualized by autoradiography. Peptides and AMPK subunits were visualized by Coomassie blue staining of the gel.

RNA extraction, reverse transcriptase-polymerase chain reaction (RT-PCR), and quantitative PCR (qPCR)

Total mRNA was extracted with TRIzol reagent (Invitrogen) and reverse-transcribed using the cDNA synthesis kit (Promega). qPCR analyses were performed as described previously[61]. The primers are listed in Supplementary Tab. 3. Calculations were performed by a comparative method ($2^{-\Delta\Delta CT}$) using 18s RNA as the internal control.

Statistical analyses

Trial experiments or experiments done previously were used to determine sample size with adequate statistical power. Quantitative results are expressed as mean ± standard error of the mean (SEM). If not stated otherwise, Student's *t* test with a two-tail distribution was performed to test for statistical significance for 2 groups. The data displayed normal variance. For more than 2 groups, one-way ANOVA with a *post-hoc* analysis using the Bonferroni test were conducted. The linear regression analysis was performed for analyzing two parameters. Statistical significance was evaluated with Graph Pad Prism 5.01. The researchers involved in the study were not blinded during sample obtainment or data analysis. Statistical significance was assumed at the 5% α-error level ($P < 0.05$).

Supplementary Material

Refer to Web version on PubMed Central for supplementary material.

ACKNOWLEDGEMENTS

We thank L. Yu for helpful discussions. We also thank D. Wang and Y. Du for technical support. This study was supported by grants to M.H. Zou (HL079584, HL080499, HL074399, HL089920, HL096032, HL105157, HL110488, and AG047776) and to Z. Xie (HL128014) from the National Institutes of Health. This study was also supported in part by grants from the National Natural Science Foundation of China (81100209, 81025002 and 91339116 to Z. Yuan and 81270355 to J. Wu), the Scientist Development Grant of American Heart Association (11SDG5560036, to P. Song), and Oklahoma Center for the Advancement of Science and Technology (HR12-061, to P. Song).

References

1. Dube JJ, et al. Effects of weight loss and exercise on insulin resistance, and intramyocellular triacylglycerol, diacylglycerol and ceramide. Diabetologia. 2011; 54:1147–1156. [PubMed: 21327867]
2. Iribarren C, Tekawa IS, Sidney S, Friedman GD. Effect of cigar smoking on the risk of cardiovascular disease, chronic obstructive pulmonary disease, and cancer in men. N Engl J Med. 1999; 340:1773–1780. [PubMed: 10362820]
3. Eliasson B, Taskinen MR, Smith U. Long-term use of nicotine gum is associated with hyperinsulinemia and insulin resistance. Circulation. 1996; 94:878–881. [PubMed: 8790020]
4. Wack JT, Rodin J. Smoking and its effects on body weight and the systems of caloric regulation. The American journal of clinical nutrition. 1982; 35:366–380. [PubMed: 7039293]
5. Flegal KM, Troiano RP, Pamuk ER, Kuczmarski RJ, Campbell SM. The Influence of Smoking Cessation on the Prevalence of Overweight in the United-States. New England Journal of Medicine. 1995; 333:1165–1170. [PubMed: 7565970]
6. Williamson DF, et al. Smoking Cessation and Severity of Weight-Gain in a National Cohort. New England Journal of Medicine. 1991; 324:739–745. [PubMed: 1997840]
7. Schnoll RA, Goren A, Annunziata K, Suaya JA. The prevalence, predictors and associated health outcomes of high nicotine dependence using three measures among US smokers. Addiction. 2013; 108:1989–2000. [PubMed: 23795712]
8. Johnson GL, Lapadat R. Mitogen-activated protein kinase pathways mediated by ERK, JNK, and p38 protein kinases. Science. 2002; 298:1911–1912. [PubMed: 12471242]
9. Rotter V, Nagaev I, Smith U. Interleukin-6 (IL-6) induces insulin resistance in 3T3-L1 adipocytes and is, like IL-8 and tumor necrosis factor-alpha, overexpressed in human fat cells from insulin-resistant subjects. J Biol Chem. 2003; 278:45777–45784. [PubMed: 12952969]
10. Hiratani K, et al. Roles of mTOR and JNK in serine phosphorylation, translocation, and degradation of IRS-1. Biochem Biophys Res Commun. 2005; 335:836–842. [PubMed: 16099428]
11. Hirosumi J, et al. A central role for JNK in obesity and insulin resistance. Nature. 2002; 420:333–336. [PubMed: 12447443]
12. Bennett BL, Satoh Y, Lewis AJ. JNK: a new therapeutic target for diabetes. Current opinion in pharmacology. 2003; 3:420–425. [PubMed: 12901952]
13. Fernandez-Galilea M, Perez-Matute P, Prieto-Hontoria PL, Martinez JA, Moreno-Aliaga MJ. Effects of lipoic acid on lipolysis in 3T3-L1 adipocytes. Journal of lipid research. 2012; 53:2296–2306. [PubMed: 22941773]
14. Heusch WL, Maneckjee R. Signalling pathways involved in nicotine regulation of apoptosis of human lung cancer cells. Carcinogenesis. 1998; 19:551–556. [PubMed: 9600337]
15. Nakamura S, et al. Nicotine induces upregulated expression of beta defensin-2 via the p38MAPK pathway in the HaCaT human keratinocyte cell line. Medical molecular morphology. 2010; 43:204–210. [PubMed: 21267696]
16. Li JM, et al. Nicotine enhances angiotensin II-induced mitogenic response in vascular smooth muscle cells and fibroblasts. Arterioscler Thromb Vasc Biol. 2004; 24:80–84. [PubMed: 14592853]
17. Salminen A, Hyttinen JM, Kaarniranta K. AMP-activated protein kinase inhibits NF-kappaB signaling and inflammation: impact on healthspan and lifespan. Journal of molecular medicine. 2011; 89:667–676. [PubMed: 21431325]

18. Steinberg GR, Kemp BE. AMPK in Health and Disease. Physiological reviews. 2009; 89:1025–1078. [PubMed: 19584320]
19. An ZB, et al. Nicotine-induced activation of AMP-activated protein kinase inhibits fatty acid synthase in 3T3L1 Adipocytes - A role for oxidant stress. Journal of Biological Chemistry. 2007; 282:26793–26801. [PubMed: 17635921]
20. Wang S, et al. Activation of AMP-activated protein kinase alpha2 by nicotine instigates formation of abdominal aortic aneurysms in mice in vivo. Nat Med. 2012; 18:902–910. [PubMed: 22561688]
21. de Morentin PBM, et al. Nicotine Induces Negative Energy Balance Through Hypothalamic AMP-Activated Protein Kinase. Diabetes. 2012; 61:807–817. [PubMed: 22315316]
22. Benowitz NL. Cigarette smoking and cardiovascular disease: pathophysiology and implications for treatment. Progress in cardiovascular diseases. 2003; 46:91–111. [PubMed: 12920702]
23. Tundulawessa Y, Yongchaiyud P, Chutrthong W, Tundulawessa K. The bioequivalent and effect of nicotine formulation gum on smoking cessation. Journal of the Medical Association of Thailand = Chotmaihet thangphaet. 2010; 93:574–579. [PubMed: 20524443]
24. Jocken JW, et al. Insulin-mediated suppression of lipolysis in adipose tissue and skeletal muscle of obese type 2 diabetic men and men with normal glucose tolerance. Diabetologia. 2013; 56:2255–2265. [PubMed: 23907381]
25. Mineur YS, et al. Nicotine Decreases Food Intake Through Activation of POMC Neurons. Science. 2011; 332:1330–1332. [PubMed: 21659607]
26. Pal D, et al. Fetuin-A acts as an endogenous ligand of TLR4 to promote lipid-induced insulin resistance. Nat Med. 2012; 18:1279–1285. [PubMed: 22842477]
27. Liew CW, et al. Ablation of TRIP-Br2, a regulator of fat lipolysis, thermogenesis and oxidative metabolism, prevents diet-induced obesity and insulin resistance. Nat Med. 2013; 19:217–226. [PubMed: 23291629]
28. Guo W, et al. Acipimox, an inhibitor of lipolysis, attenuates atherogenesis in LDLR-null mice treated with HIV protease inhibitor ritonavir. Arterioscler Thromb Vasc Biol. 2009; 29:2028–2032. [PubMed: 19762785]
29. Hardie DG, Ross FA, Hawley SA. AMPK: a nutrient and energy sensor that maintains energy homeostasis. Nature reviews. Molecular cell biology. 2012; 13:251–262. [PubMed: 22436748]
30. Fullerton MD, et al. Single phosphorylation sites in Acc1 and Acc2 regulate lipid homeostasis and the insulin-sensitizing effects of metformin. Nat Med. 2013; 19:1649–1654. [PubMed: 24185692]
31. Ruderman NB, Carling D, Prentki M, Cacicedo JM. AMPK, insulin resistance, and the metabolic syndrome. J Clin Invest. 2013; 123:2764–2772. [PubMed: 23863634]
32. Musi N, et al. AMP-activated protein kinase (AMPK) is activated in muscle of subjects with type 2 diabetes during exercise. Diabetes. 2001; 50:921–927. [PubMed: 11334434]
33. Garton AJ, et al. Phosphorylation of bovine hormone-sensitive lipase by the AMP-activated protein kinase. A possible antilipolytic mechanism. European journal of biochemistry / FEBS. 1989; 179:249–254. [PubMed: 2537200]
34. Daval M, et al. Anti-lipolytic action of AMP-activated protein kinase in rodent adipocytes. J Biol Chem. 2005; 280:25250–25257. [PubMed: 15878856]
35. Bourron O, et al. Biguanides and thiazolidinediones inhibit stimulated lipolysis in human adipocytes through activation of AMP-activated protein kinase. Diabetologia. 2010; 53:768–778. [PubMed: 20043143]
36. Djouder N, et al. PKA phosphorylates and inactivates AMPKalpha to promote efficient lipolysis. EMBO J. 2010; 29:469–481. [PubMed: 19942859]
37. Ahmadian M, et al. Desnutrin/ATGL is regulated by AMPK and is required for a brown adipose phenotype. Cell Metab. 2011; 13:739–748. [PubMed: 21641555]
38. Lin L, et al. Adipocyte expression of PU.1 transcription factor causes insulin resistance through upregulation of inflammatory cytokine gene expression and ROS production. Am J Physiol Endocrinol Metab. 2012; 302:E1550–E1559. [PubMed: 22454293]
39. Um SH, et al. Absence of S6K1 protects against age- and diet-induced obesity while enhancing insulin sensitivity. Nature. 2004; 431:200–205. [PubMed: 15306821]

40. Horike N, et al. Adipose-specific expression, phosphorylation of Ser794 in insulin receptor substrate-1, and activation in diabetic animals of salt-inducible kinase-2. J Biol Chem. 2003; 278:18440–18447. [PubMed: 12624099]
41. Sanchez-Tillo E, et al. JNK1 Is required for the induction of Mkp1 expression in macrophages during proliferation and lipopolysaccharide-dependent activation. J Biol Chem. 2007; 282:12566–12573. [PubMed: 17337450]
42. Brondello JM, Pouyssegur J, McKenzie FR. Reduced MAP kinase phosphatase-1 degradation after p42/p44MAPK-dependent phosphorylation. Science. 1999; 286:2514–2517. [PubMed: 10617468]
43. Wu JJ, et al. Mice lacking MAP kinase phosphatase-1 have enhanced MAP kinase activity and resistance to diet-induced obesity. Cell Metab. 2006; 4:61–73. [PubMed: 16814733]
44. Zhong C, Talmage DA, Role LW. Nicotine elicits prolonged calcium signaling along ventral hippocampal axons. PLoS One. 2013; 8:e82719. [PubMed: 24349346]
45. Hogg RC, Bertrand D. Neuroscience. What genes tell us about nicotine addiction. Science. 2004; 306:983–985. [PubMed: 15528431]
46. Friedman TC, et al. Additive effects of nicotine and high-fat diet on hepatic steatosis in male mice. Endocrinology. 2012; 153:5809–5820. [PubMed: 23093702]
47. Seoane-Collazo P, et al. Nicotine improves obesity and hepatic steatosis and ER stress in diet-induced obese male rats. Endocrinology. 2014; 155:1679–1689. [PubMed: 24517227]
48. Xu TY, et al. Chronic Exposure to Nicotine Enhances Insulin Sensitivity through alpha 7 Nicotinic Acetylcholine Receptor-STAT3 Pathway. Plos One. 2012; 7
49. Yoon MJ, et al. Adiponectin increases fatty acid oxidation in skeletal muscle cells by sequential activation of AMP-activated protein kinase, p38 mitogen-activated protein kinase, and peroxisome proliferator-activated receptor alpha. Diabetes. 2006; 55:2562–2570. [PubMed: 16936205]
60. Lin YW, Yang JL. Cooperation of ERK and SCFSkp2 for MKP-1 destruction provides a positive feedback regulation of proliferating signaling. J Biol Chem. 2006; 281:915–926. [PubMed: 16286470]
51. Choi SM, et al. Insulin regulates adipocyte lipolysis via an Akt-independent signaling pathway. Mol Cell Biol. 2010; 30:5009–5020. [PubMed: 20733001]
52. Villena JA, et al. Induced adiposity and adipocyte hypertrophy in mice lacking the AMP-activated protein kinase-alpha2 subunit. Diabetes. 2004; 53:2242–2249. [PubMed: 15331533]
53. Bolinder J, Sjoberg S, Arner P. Stimulation of adipose tissue lipolysis following insulin-induced hypoglycaemia: evidence of increased beta-adrenoceptor-mediated lipolytic response in IDDM. Diabetologia. 1996; 39:845–853. [PubMed: 8817110]
54. Wolffenbuttel BH, Weber RF, van Koetsveld PM, Weeks L, Verschoor L. A randomized crossover study of sulphonylurea and insulin treatment in patients with type 2 diabetes poorly controlled on dietary therapy. Diabetic medicine : a journal of the British Diabetic Association. 1989; 6:520–525. [PubMed: 2527134]
55. Gabrielsson J, Bondesson U. Constant-rate infusion of nicotine and cotinine. I. A physiological pharmacokinetic analysis of the cotinine disposition, and effects on clearance and distribution in the rat. Journal of pharmacokinetics and biopharmaceutics. 1987; 15:583–599. [PubMed: 3450843]
56. Song P, et al. Adenosine monophosphate-activated protein kinase-alpha2 deficiency promotes vascular smooth muscle cell migration via S-phase kinase-associated protein 2 upregulation and E-cadherin downregulation. Arterioscler Thromb Vasc Biol. 2013; 33:2800–2809. [PubMed: 24115035]
57. Dorfman K, et al. Disruption of the erp/mkp-1 gene does not affect mouse development: normal MAP kinase activity in ERP/MKP-1-deficient fibroblasts. Oncogene. 1996; 13:925–931. [PubMed: 8806681]
58. Blattler SM, et al. Yin Yang 1 deficiency in skeletal muscle protects against rapamycin-induced diabetic-like symptoms through activation of insulin/IGF signaling. Cell Metab. 2012; 15:505–517. [PubMed: 22482732]
59. Turner N, et al. Distinct patterns of tissue-specific lipid accumulation during the induction of insulin resistance in mice by high-fat feeding. Diabetologia. 2013; 56:1638–1648. [PubMed: 23620060]

60. Li P, et al. Adipocyte NCoR knockout decreases PPARgamma phosphorylation and enhances PPARgamma activity and insulin sensitivity. Cell. 2011; 147:815–826. [PubMed: 22078880]
61. Zhang W, Wang Q, Song P, Zou MH. Liver kinase b1 is required for white adipose tissue growth and differentiation. Diabetes. 2013; 62:2347–2358. [PubMed: 23396401]
62. Targher G, et al. Cigarette smoking and insulin resistance in patients with noninsulin-dependent diabetes mellitus. Journal of Clinical Endocrinology & Metabolism. 1997; 82:3619–3624. [PubMed: 9360516]
63. Coburn CT, et al. Defective uptake and utilization of long chain fatty acids in muscle and adipose tissues of CD36 knockout mice. J Biol Chem. 2000; 275:32523–32529. [PubMed: 10913136]
64. Siri P, et al. Post-transcriptional stimulation of the assembly and secretion of triglyceride-rich apolipoprotein B lipoproteins in a mouse with selective deficiency of brown adipose tissue, obesity, and insulin resistance. J Biol Chem. 2001; 276:46064–46072. [PubMed: 11598138]
65. Wang S, Song P, Zou MH. Inhibition of AMP-activated protein kinase alpha (AMPKalpha) by doxorubicin accentuates genotoxic stress and cell death in mouse embryonic fibroblasts and cardiomyocytes: role of p53 and SIRT1. J Biol Chem. 2012; 287:8001–8012. [PubMed: 22267730]
66. Xie ZL, et al. Identification of the Serine 307 of LKB1 as a Novel Phosphorylation Site Essential for Its Nucleocytoplasmic Transport and Endothelial Cell Angiogenesis. Molecular and Cellular Biology. 2009; 29:3582–3596. [PubMed: 19414597]

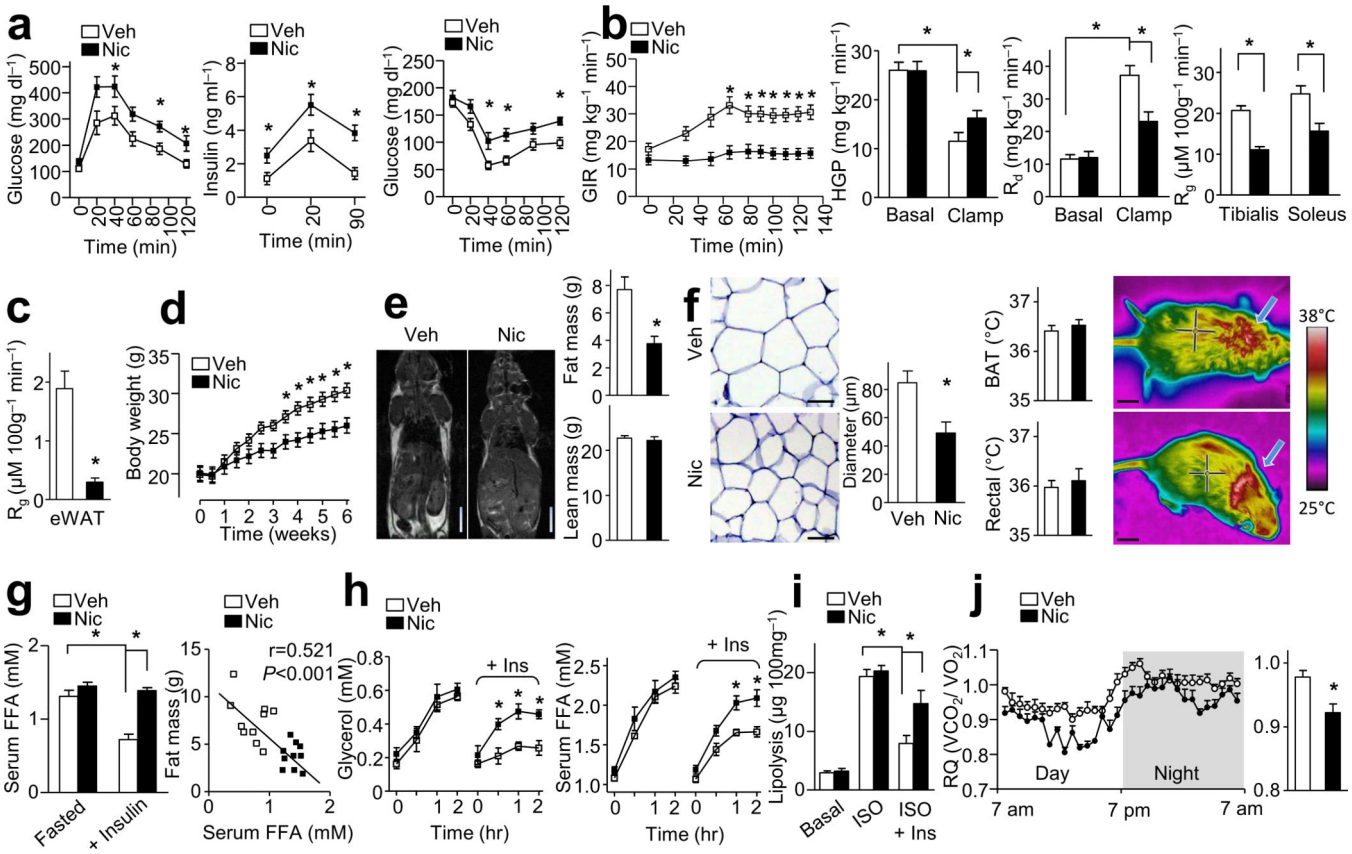

Figure 1.

Nicotine (Nic) perfusion induces IR and lower adiposity. (**a**) IPGTT, insulin release, and ITT; *n* = 10–11 each. (**b,c**) Hyperinsulinemic-euglycemic (H-E) clamp. Glucose infusion rate (GIR), hepatic glucose production (HGP), the rate of the disappearance (R_d) and the glucose metabolic index (R_g) in tibialis anterior and soleus (**b**) or epididymal white adipose tissue (eWAT, **c**); *n* = 9 each. (**d**) Body weight changes; *n* = 11 each. (**e**) Representative MRI images (*n* = 4 each) for fat distribution, fat mass and lean mass (*n* = 11 each). Scale bars, 1 cm. (**f**) Representative eWAT sections (*n* = 10 sections each) and quantification of adipocyte diameter (Scale bars, 50 μm, *n* = 10 each), and temperature of brown adipose tissue (BAT) area and rectal temperature (*n* = 10 each) with representative infrared thermal images (Scale bars, 1 cm). (**g**) Serum FFA after overnight fasting or insulin perfusion at 40 min during ITT (*n* = 10 each), and the linear regression between fat mass and serum FFA levels during insulin perfusion (*n* = 10 each). (**h**) *In vivo* lipolysis. (*n* = 8 each). (**i**) In vitro lipolysis assay of isolated adipocytes; *n* = 7 each. (**j**) Respiratory quotients (RQ, VCO_2/ VO_2) (left) and the average data (right). *n* = 10 each. Significance determined by one-way ANOVA with repeated measures for the inter-assay evaluations (**a,b,d,h**), Student's *t*-test (**c,e,f,j**), one-way ANOVA with Bonferroni's *post-hoc* test (**g,i**) and **P* < 0.05. All values are means ± SEM.

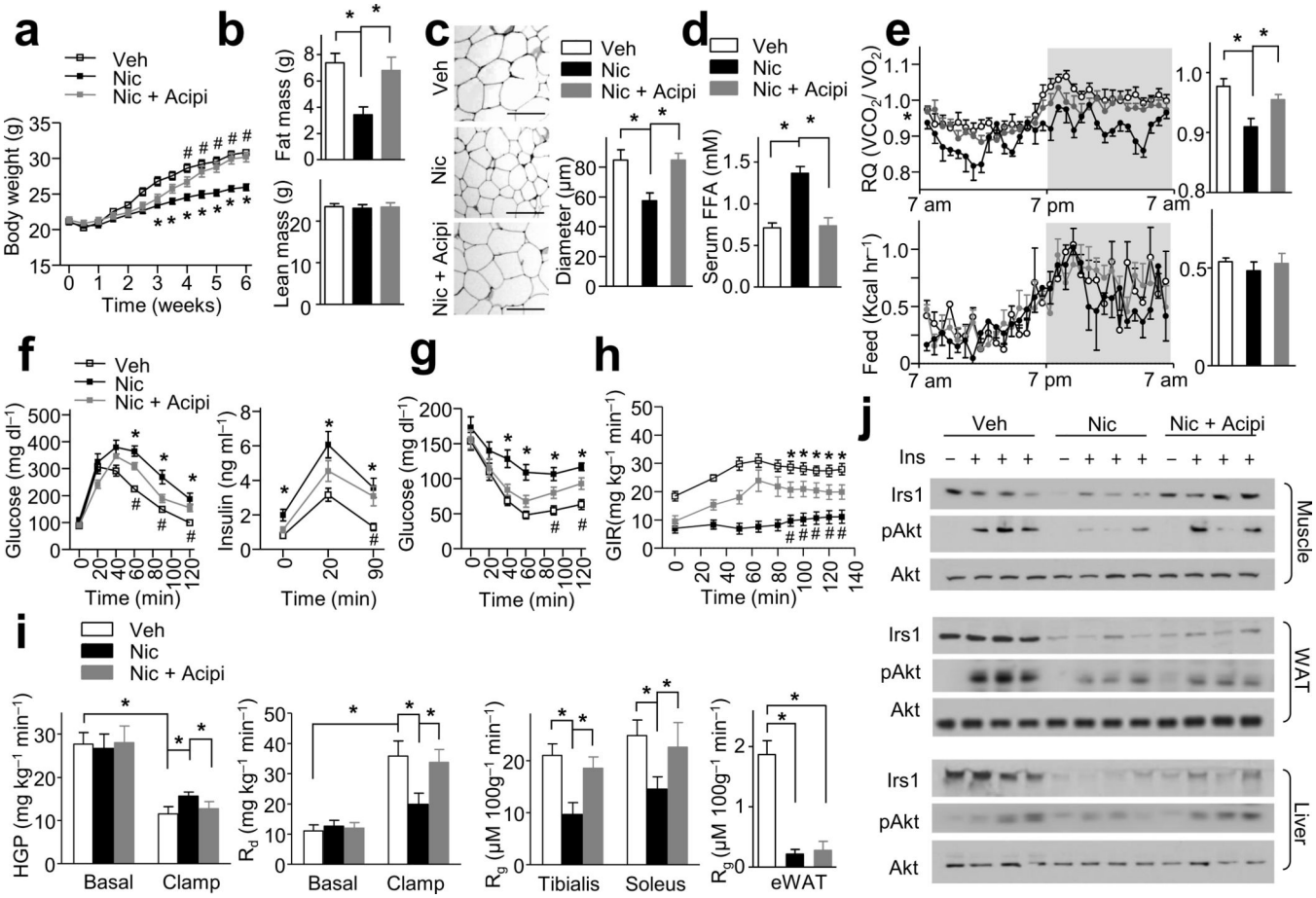

Figure 2.

Lipolysis inhibition blocks nicotine-induced IR and adiposity reduction. Wild-type mice were treated with Nic, vehicle (Veh) or Nic + acipimox (Nic + Acipi). (**a**) Body weight changes; *n* = 8–9 each. (**b**) Fat mass and lean mass; *n* = 8–9 each. (**c**) Representative H&E-stained WAT sections (*n* = 10 sections each) and the diameters of adipocytes in WAT (Scale bar, 100 μm); *n* = 8–9 each. (**d**) Serum FFA levels in insulin-perfused mice (at 40 min during ITT); *n* = 8 each. (**e**) The respiratory quotients (RQ, VCO_2/VO_2) and food intake (feed) during light and dark cycles, as indicated by the white and gray areas (average data in the right panels); *n* = 6 each. (**f,h**) IPGTT, insulin release, ITT data; *n* = 8–9 each. (**i**) H-E clamp (*n* = 8 each). Glucose infusion rate (GIR), hepatic glucose production (HGP), the rate of the disappearance (R_d), and the glucose metabolic index (R_g) in tibialis anterior and soleus muscles or eWAT. (**j**) Irs1 and Akt signaling in muscle, liver and WAT; *n* = 8 each. Significance determined by one-way ANOVA with repeated measures for the inter-assay evaluations (**a,f,g,h**), one-way ANOVA with Bonferroni's *post-hoc* test (**b,c,d,e,i**), $^{*}P < 0.05$ (Veh vs. Nic), $^{\#}P < 0.05$ (Nic vs. Nic + Acpi. All values are means ± SEM.

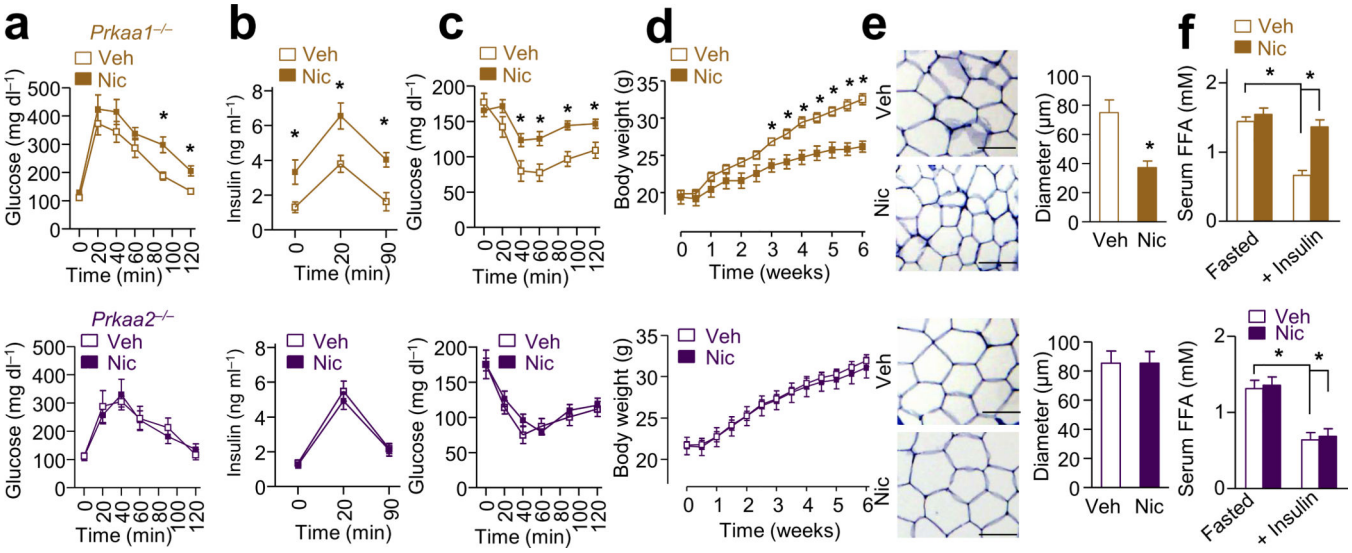

Figure 3.

Deletion of AMPKα2, but not AMPKα1, blocks nicotine-induced IR and inhibition of weight gain in mice. Nic or Veh was perfused by minipump in wild type (WT), *Prkaa1*$^{-/-}$, or *Prkaa2*$^{-/-}$ mice. (**a–c**) IPGTT, insulin release, and ITT in mice; n = 8–10 each. (**d**) Body weight changes; n = 8–10 each. (**e**) Representative images of WAT sections (n = 10 sections each) analyzing cell sizes and the adipocyte diameter (Scale bar, 100 μm); n = 8 each. (**f**) Serum FFA levels after overnight fasting (Fasted) or insulin perfusion (at 40 min during ITT); n = 8 each. Significance determined by one-way ANOVA with repeated measures for the inter-assay evaluations (**a,b,c,d**), Student's *t*-test (**e**), one-way ANOVA with Bonferroni's *post-hoc* test (**f**) and *$P < 0.05$. All values are means ± SEM.

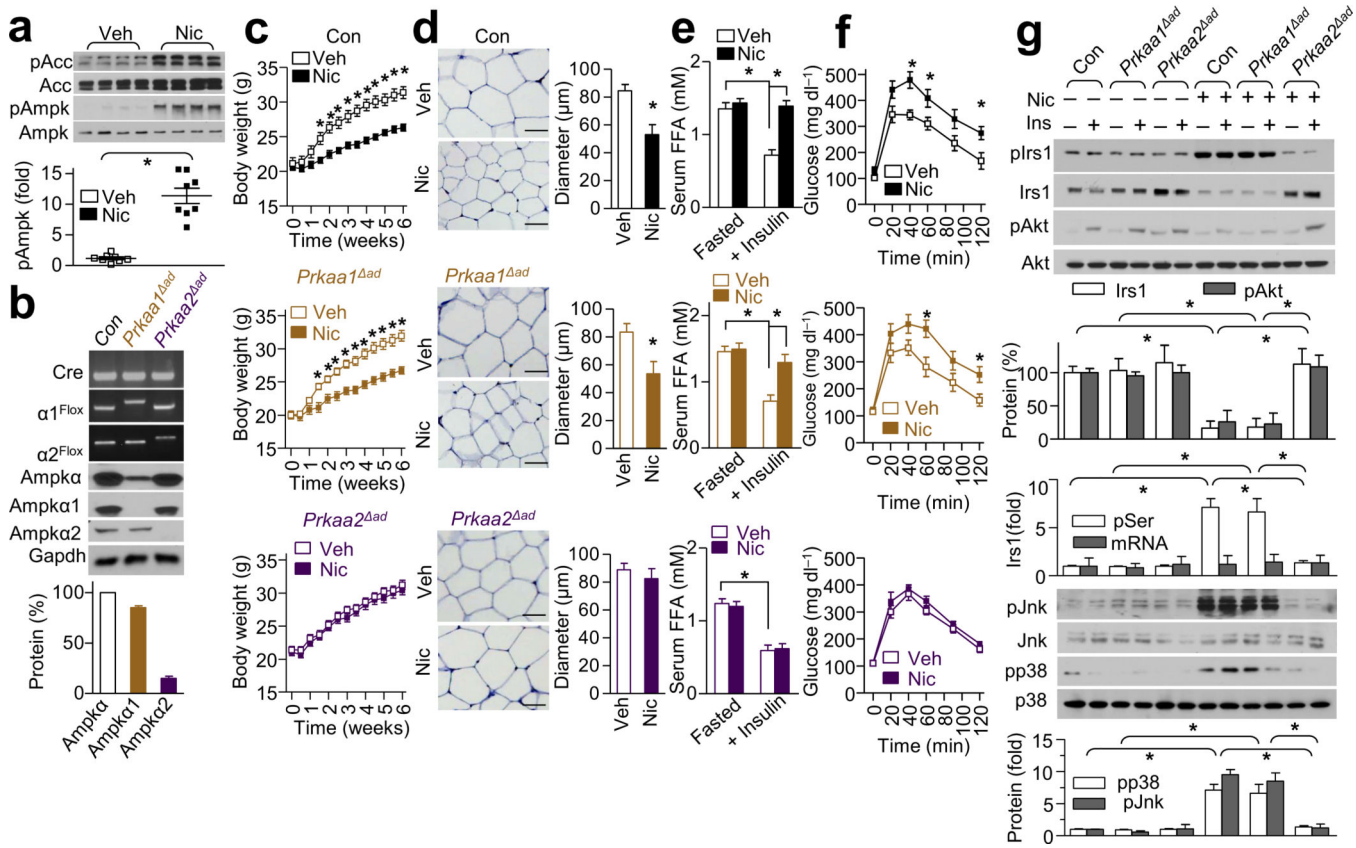

Figure 4.

Adipose AMPKα2 is required for the nicotine-dependent inhibitory effects on weight gain and insulin signaling in mice. Nic or Veh was perfused in control (Con, black), *Prkaa1*$^{\Delta ad}$ (brown) and *Prkaa2*$^{\Delta ad}$ (purple) mice. (**a**) Phosphorylated AMPK at Thr172 (pAMPK) and phosphorylated ACC (pACC) expression in WAT; $n = 8$ each. (**b**) Genotypes of adipose-specific knockout mice and the expressions of AMPKα, AMPKα1, and AMPKα2 in isolated adipocytes; $n = 8$ each. (**c**) Body weight in mice perfused with Veh or Nic; $n = 8$–9 each. (**d**) Representative H&E-stained WAT sections ($n = 10$ section each) and the diameters of adipocytes in WAT (Scale bar, 50 μm); $n = 8$ each. (**e**) Serum FFA levels after overnight fasting (Fasted) or insulin perfusion at 40 min during ITT; $n = 8$ each. (**f**) IPGTT in mice treated with Veh or Nic; $n = 8$–9 each. (**g**) Irs1, pIrs1-Ser307 (pIrs1), pAkt-Ser473 (pAkt), p38, and JNK signaling in WAT of mice injected with saline or insulin (1 unit kg^{-1}); $n = 8$ each. Significance determined by Student's *t*-test (**a,d**), one-way ANOVA with repeated measures for the inter-assay evaluations (**c,f**), one-way ANOVA with Bonferroni's *post-hoc* test (**e,g**) and $^*P < 0.05$. All values are means ± SEM.

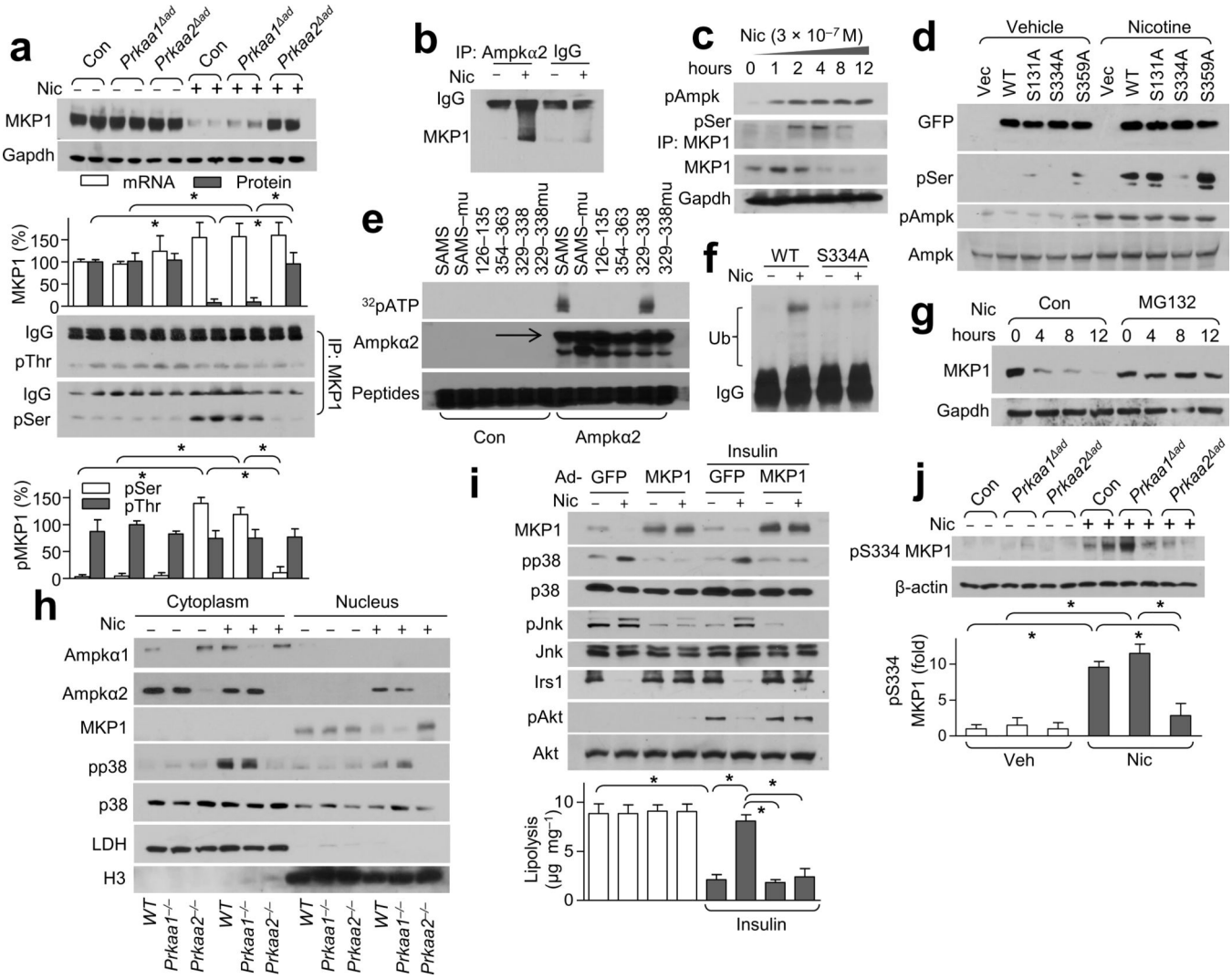

Figure 5.

Nicotine treatment results in greater pMKP1-Ser334 levels and subsequent degradation through AMPK. (**a**) MKP1 expression (top) and its serine (Ser) /threonine (Thr) phosphorylation (bottom) in WAT from Veh- or Nic-treated mice. Gapdh was detected as a loading control; *n* = 8 each. (**b**) AMPKα2-MKP1binding in MEF-derived adipocytes; *n* = 5 each. (**c**) AMPK activation and MKP1 serine phosphorylation in nicotine-treated isolated adipocytes; *n* = 4 each. (**d**) MKP1 phosphorylation in HEK293 cells transfected with vector, GFP-tagged WT MKP1 (WT) or the indicated site-directed mutants of MKP1; *n* = 4 each. (**e**) The indicated peptides (the SAMS peptide and its mutant, SAMSmu) or peptides spanning the indicated amino acid residues of MKP1; *n* = 3 each. (**f**) MKP1 ubiquitination in HEK293 cells transfected with WT MKP1 (WT) or MKP1-S334A; *n* = 4 each. (**g**) MKP1 protein expression in MG132-treated isolated adipocytes; *n* = 5 each. (**h**) The subcellular localization of AMPKα1/2, p38 and MKP1 in adipocytes treated with or without nicotine. LDH (lactate dehydrogenase), cytoplasmic marker; H3 (histone 3), nuclear marker; *n* = 5 each. (**i**) Insulin signaling (western blot, top) and lipolysis (bottom) in Nic- or Veh-treated MEF-derived adipocytes transfected with adenovirus GFP (Ad-GFP) or MKP1 (Ad-

MKP1).; $n = 5$ each. (**j**) Detection of pMKP1-S334 in WAT from the indicated strains in Nic- or Veh-treated mice (top) and its quantitation (bottom). Beta-actin was detected as a loading control; $n = 6$ each. Significance determined by one-way ANOVA with Bonferroni's *post-hoc* test (**a,i,j**) and $*P < 0.05$. All values are means ± SEM.

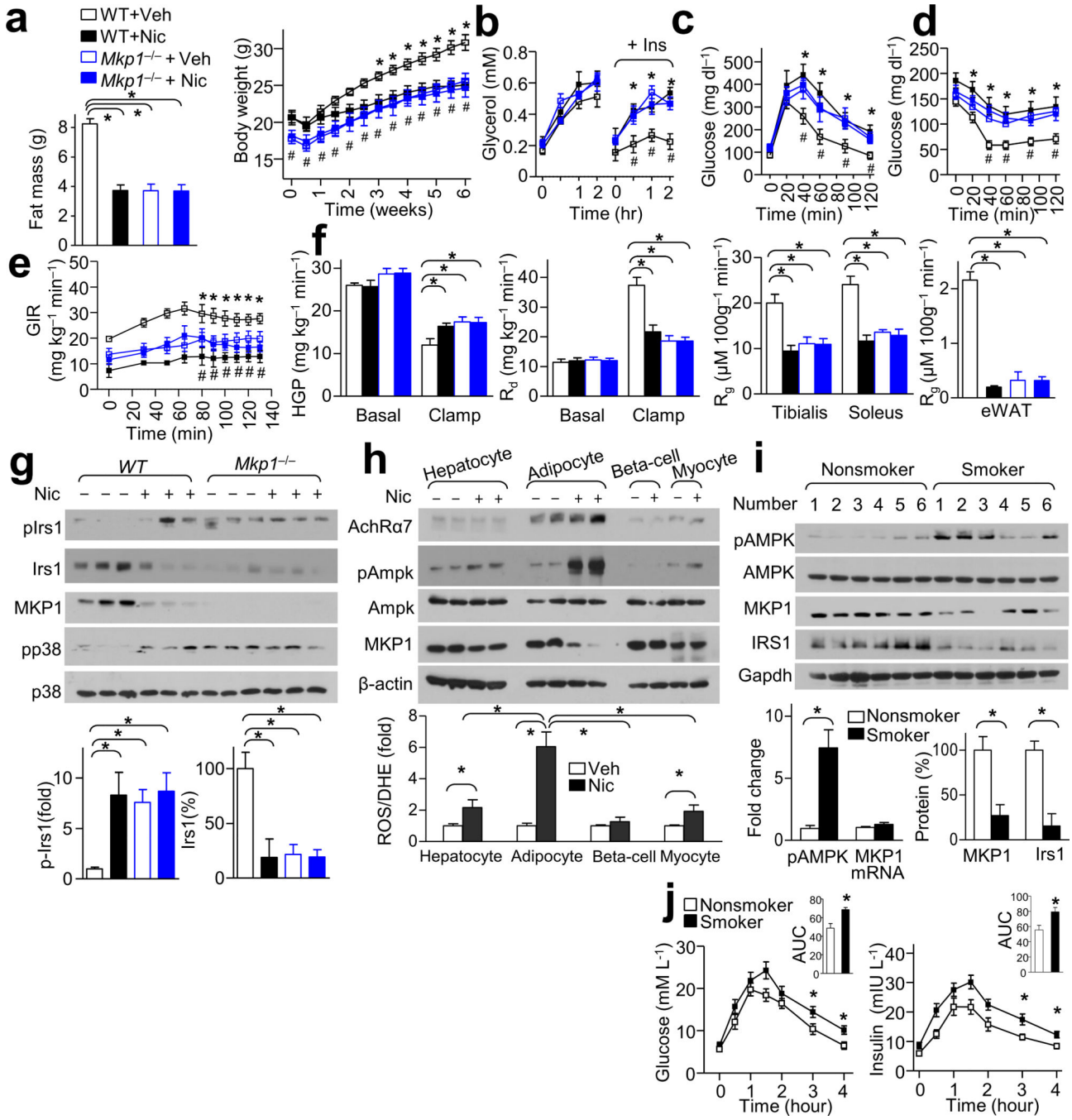

Figure 6.

MKP1 reduction is required for nicotine-mediated IR and lipolysis. (**a–g**) WT and *Mkp1*$^{-/-}$ mice were treated with Veh or Nic. (**a**) Body weight changes and fat mass in mice treated with Veh or Nic; n = 7–8 each. (**b**) In vivo lipolysis. Plasma glycerol concentration measured at 0, 15, 60, 120 min; n = 6 each. (**c,d**) IPGTT (**c**) and ITT (**d**) data in mice; n = 7–8 each. (**e,f**) The glucose infusion rate (GIR) (**e**) and the hepatic glucose production (HGP), the rate of the disappearance (R_d) and in tibialis anterior and soleus muscles or eWAT the glucose metabolic index (R_g) (**f**) during a hyperinsulinemic-euglycemic clamp (n = 6 each).

(**g**) MKP1, pIrs1- Ser307, Irs1 and p38 signaling in WAT of mice of the indicated genotype; $n = 6$ each. (**h**) AchRα7 expression in isolated adipocytes, hepatocytes, β-cells, and myocytes after treatment with Nic or Veh; $n = 6$ each. (**i**) Detection of pAMPK, AMPK, MKP1, and Irs1 expression in WAT in smokers and nonsmokers; $n = 12$ each. (**j**) Oral glucose tolerance test (OGTT) (left), the insulin levels during OGTT (right) and the areas under the curve (AUC); $n = 12$ each. Significance determined by one-way ANOVA with Bonferroni's *post-hoc* test (**a,f,g,j**), one-way ANOVA with repeated measures for the inter-assay evaluations (**b,c,d,e**), Student's *t*-test (**h,i**), $^{*}P < 0.05$ Veh vs.Nic, and $^{\#}P < 0.05$ *WT* vs. *Mkp1*$^{-/-}$ mice. All values are means ± SEM.